SANDIA REPORT
SAND2019-7760
Printed June 2019

Sandia National Laboratories

Multigroup Neutron Cross Section Generation for the SCEPTRE Code

Donald E. Bruss, Lawrence C. Sanchez

Prepared by
Sandia National Laboratories
Albuquerque, New Mexico
87185 and Livermore,
California 94550

Issued by Sandia National Laboratories, operated for the United States Department of Energy by National Technology & Engineering Solutions of Sandia, LLC.

Available to DOE and DOE contractors from
U.S. Department of Energy
Office of Scientific and Technical Information
P.O. Box 62
Oak Ridge, TN 37831

Telephone: (865) 576-8401
Facsimile: (865) 576-5728
E-Mail: reports@osti.gov
Online ordering: http://www.osti.gov/scitech

Available to the public from
U.S. Department of Commerce
National Technical Information Service
5301 Shawnee Rd
Alexandria, VA 22312

Telephone: (800) 553-6847
Facsimile: (703) 605-6900
E-Mail: orders@ntis.gov
Online order: https://classic.ntis.gov/help/order-methods/

ABSTRACT

Multigroup neutron cross sections were generated for the deterministic radiation transport code SCEPTRE. ENDF/B-VII.1 nuclear data files were downloaded from Los Alamos National Laboratory (LANL), processed with the LANL cross-section preparation code NJOY-2012, and post-processed to produce a SCEPTRE-formatted cross section file.

A simple radiation transport problem was used to compare results calculated with MCNP, a continuous-energy radiation transport code from LANL, to results calculated with SCEPTRE using the NJOY-2012-produced multigroup cross sections. This problem was used to debug the python scripts used to post-process the NJOY-2012 output and to assess the accuracy of the multigroup cross sections.

These comparisons demonstrate that the multigroup cross sections generated in this work are accurate for most elements but yielded inaccurate results for several common transition metals. This discrepancy appears to result from poor treatment of the resolved resonance region of the continuous-energy cross sections. Further work is recommended to investigate alternative methods to treat these resonances with NJOY-2012.

This page left blank

CONTENTS

LIST OF FIGURES

LIST OF TABLES

ACRONYMS AND DEFINITIONS

Abbreviation	Definition
ENDF	Evaluated Nuclear Data File; a format for cross-section data.
ENDF/B-VII.1	Version VII.1 of neutron cross section data in the ENDF/B data format.
LANL	Los Alamos National Laboratory
MCNP	The Los Alamos National Laboratory Monte Carlo Neutral Particle code; a Monte Carlo radiation transport code.
NJOY-2012	A Los Alamos National Laboratory code to process nuclear data in the ENDF/B data format to produce multigroup cross sections.
SCEPTRE	The Sandia Computational Engine for Particle Transport for Radiation Effects; a deterministic radiation transport code.

1. NUCLEAR CROSS-SECTIONS

The Sandia Computational Engine for Particle Transport for Radiation Effects (SCEPTRE) radiation transport code solves the Boltzmann equation for particle transport,

$$\frac{d}{dt}\psi(\vec{r},\vec{\Omega},E) + \vec{\Omega}\cdot\vec{\nabla}\psi(\vec{r},\vec{\Omega},E) + \sigma_t(\vec{r},E)\psi(\vec{r},\vec{\Omega},E) = \int dE' \int d\Omega' \sigma_s(\vec{r},E'\rightarrow E,\vec{\Omega}'\cdot\vec{\Omega})\psi(\vec{r},\vec{\Omega}',E') + q(\vec{r},\vec{\Omega},E).$$

The angular flux variable ψ describes the radiation field as a function of space $\vec{r}$, angle $\vec{\Omega}$, and energy E. The first term in the Boltzmann equation corresponds to the time dependence of the radiation field. The second term describes radiation streaming. The third captures the interaction of radiation with the background material through the total cross section, σ_t. The fourth term characterizes interactions in which particles change energy or direction, interactions which are characterized by the scattering cross section σ_s. The final term represents sources of radiation. This seven-dimensional partial differential equation is discretized in space (three dimensions) by the method of finite elements, in angle (two dimensions) by the discrete ordinates (S_N) approximation, and in energy (one dimension) by the multigroup method. For many applications a steady-state solution is required, removing one dimension (time). (E. E. Lewis and W. F. Miller, 1993).

The Boltzmann transport equation is applicable to both neutral and charged particles (although the above equation neglects terms involving electric or magnetic fields). The SCEPTRE transport code is particle-agnostic but is primarily applied to coupled photon-electron radiation transport problems. Given appropriate cross-section data SCEPTRE may be applied to any particle species for which the Boltzmann equation is applicable.

Cross-section data characterize the interaction of radiation with matter. These interactions depend upon the material with which the radiation interacts and upon the radiation energy. Photons and electrons primarily interact with the electrons orbiting nuclei. Cross sections for photons and electrons are therefore computed on an element-by-element basis. Neutrons interact with nuclei and therefore are isotope-specific; neutron cross sections for elements and materials must be calculated for each isotope present in the material and then combined according to isotopic abundances. The spatial dependence of the cross-section terms in the Boltzmann equation is usually handled by mapping spatial positions to material identities and using the cross sections corresponding to the identified material.

Radiation may collide with the background material through a variety of interactions. Radiation particles may change direction and/or energy or be absorbed in a given interaction. The particles may deposit energy or create secondary particles as part of that interaction. All possible interactions must be modeled in the cross-section data to accurately model the particle's behavior. These interactions are strongly dependent upon the energy of the radiation (the velocity of a neutron or electron or frequency of a photon).

Cross-section data may be both measured experimentally and calculated from numerical models. Evaluated cross-section data files are compiled by subject-matter experts and combine data from numerous experimental and numerical data sets, usually including best estimates of uncertainty

in the compiled data. These data sets approximate the continuous-energy cross sections with data points and suggested interpolations schemes to characterize smoothly-varying data and parameters which are used to reconstruct discontinuous or rapidly-varying features in the cross sections. These data sets may be stored in a standardized data format called the Evaluated Nuclear Data Files (ENDF).

Photon and electron cross sections exhibit smoothly-varying regions interrupted by discontinuous jumps in the interaction probability. These discontinuities correspond to threshold energies above which additional interactions are energetically possible (binding energies). The total cross section, which conveys the probability of undergoing any interaction with the background material, for photons interacting with lead is plotted in Figure 1.

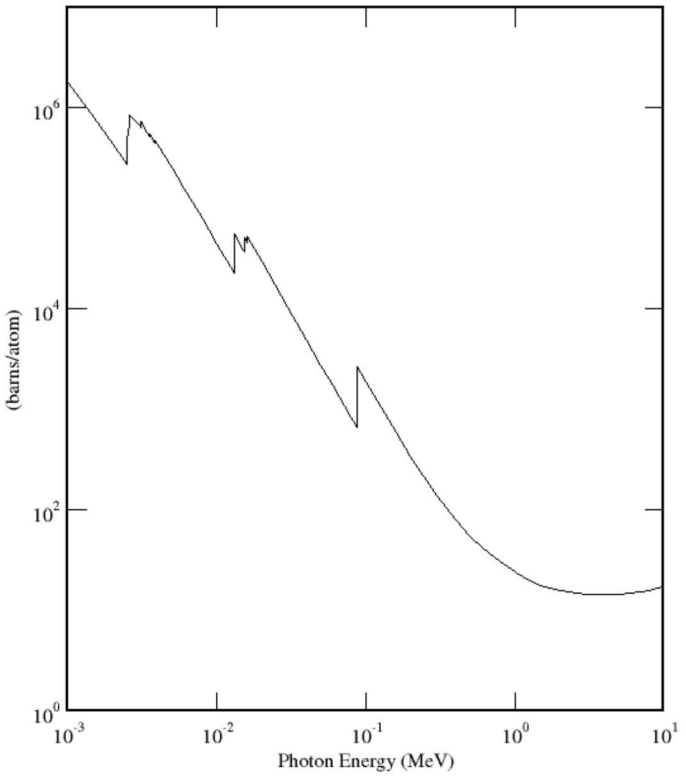

Figure 1: Total photon cross section for lead. (National Institute of Standards and Technology Physical Measurement Laboratory, 2019)

Neutron cross sections exhibit strong discontinuities in energy. These "resonances" drastically complicate the modeling of neutron interactions. The total neutron, absorption, elastic scattering, and gamma production cross section for gold, which is naturally mono-isotopic (Au-197), is plotted in Figure 2.

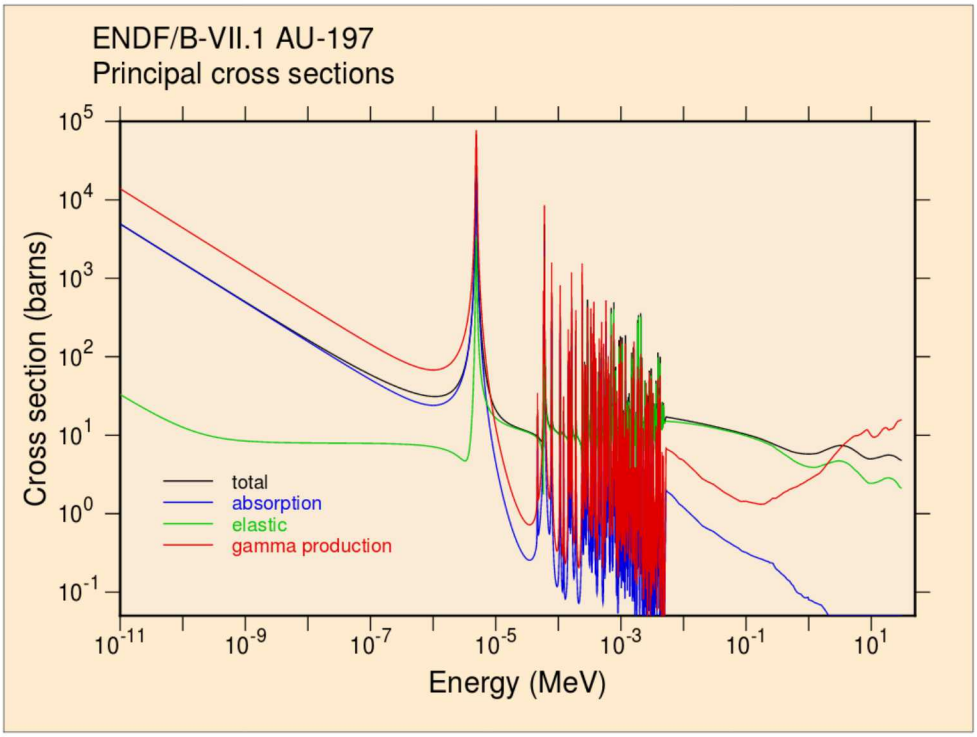

Figure 2: Total and constituent neutron cross sections for gold, Au-197 (ENDF-VII.1). (Los Alamos National Laboratory T-2 Nuclear Information Service, 2019)

Many interactions create secondary particles. These particles may be of the same species as the parent particle, such as (n,2n) reactions, or they may be of a different species, such as photons undergoing photo-ionization liberating an electron and then additional photons through relaxation. Several neutron interactions produce gamma rays through absorption or inelastic scattering. Depending upon the problem of interest many cross-section generation codes create coupled cross-section sets that include multiple particle species.

While photon and electron cross sections are challenging to measure below about 1keV because of the negligible range of these particles at low energies (as is clear in Figure 1), neutron cross sections extend to small fractions of an eV. At low energies neutrons will come into thermal equilibrium with the background material-that is, eventually, neutrons will not lose energy by scattering because the kinetic energy of the background material prevents the neutrons from down-scattering any further (Duderstadt, 1976). Additionally, at very low energies neutrons may interact not just with individual nuclei but with molecules (such as water) or lattices of nuclei (such as graphite).

2. MULTIGROUP CROSS SECTIONS

In this section the theory of multigroup cross sections is introduced, the generation of these cross sections with the cross-section preparation code NJOY-2012 is outlined, and the work necessary to post-process the NJOY-2012 output and prepare the multigroup cross sections for use by SCEPTRE is explained.

2.1. Theory of multigroup cross sections

Deterministic radiation transport codes discretize the energy variable according to the multigroup method. The Boltzmann equation is solved in discrete energy groups creating a series of coupled PDEs. A piecewise-constant approximation of the continuous-energy cross sections is calculated to preserve the average cross section within each group,

$$\sigma_{\{t,g\}} = \frac{\int_{E_{g-1}}^{E_g} \sigma_t(E) w(E)\, dE}{\int_{E_{g-1}}^{E_g} w(E)\, dE}.$$

Here $\sigma_{\{t,g\}}$ is the total cross section in group g, energies E_{g-1} and E_g correspond to the lower and upper bounds of energy group g, respectively, and w(E) is a weighting function (R.E. MacFarlane, 2012). The choice of the weighting function can be quite complicated. For very fine group structures (such that the cross section is slowly-varying over the width of each energy group) a constant weighting function may be used without introducing error. For smoothly-varying regions of cross sections, simple weighting functions yield accurate cross sections. However, the edges visible in the photon cross sections in Figure 1 and resonances visible in the neutron cross sections in Figure 2 require carefully-chosen weighting spectra due to energy self-shielding effects (E. E. Lewis and W. F. Miller, 1993).

The correct weighting spectrum to use when calculating cross sections is the continuous-energy scalar flux $\phi(\vec{r},E)$ (that is, the angular flux integrated over angular direction) solution to the problem for which the cross sections are needed,

$$\sigma_{\{t,g\}}(\vec{r}) = \frac{\int_{E_{g-1}}^{E_g} \sigma_t(\vec{r},E)\phi(\vec{r},E)\, dE}{\int_{E_{g-1}}^{E_g} \phi(\vec{r},E)\, dE}.$$

Because the scalar flux depends upon position $\vec{r}$ in addition to energy the cross sections should also depend upon position and not just material identity. In practice, the weighting spectrum used to

generate multigroup cross sections is usually approximated by a representative scalar flux, $\phi(E)$, that characterizes the energy-dependent behavior of the full angular flux solution to the problem of interest or a simplified problem related to the problem of interest. The energy-dependent scalar flux will show strong depressions in the immediate vicinity (in energy) of strong resonances in the cross sections. These depressions greatly impact the weighted cross sections generated by evaluating this integral (R.E. MacFarlane, 2012). For many applications, a simple physics-informed weighting function is sufficient to generate accurate cross sections, but accurately generating cross sections for materials with strong resonances can be very challenging.

The anisotropic behavior of radiation interactions is captured in discrete-ordinates transport codes by representing the scattering term in the Boltzmann equation as the sum of Legendre polynomials in angle. Moments of the scattering cross sections are calculated in a similar fashion to the scattering cross section above (R.E. MacFarlane, 2012).

2.2. Multigroup cross section generation with NJOY-2012

Although SCEPTRE is particle-agnostic the ability to generate multigroup neutron cross sections for SCEPTRE has not existed for many years. Multigroup photon-electron cross sections are generated with the CEPXS code from Sandia National Laboratories. Although multigroup neutron cross sections have been provided to SCEPTRE in the past this capability has not been exercised in many years.

The code NJOY-2012 from Los Alamos National Laboratory is used to process nuclear data in the ENDF/B format to produce multigroup cross sections (R.E. MacFarlane, 2012). Nuclear data in this format is publicly available through repositories of the ENDF/B-VII.1 data at Los Alamos National Laboratory (Los Alamos National Laboratory T-2 Nuclear Information Service, 2019). NJOY-2012 may be used to generate cross sections in a variety of formats for both deterministic and Monte Carlo transport codes. The process used to generate multigroup cross sections by applying NJOY-2012 to ENDF/B-VII.1 data files is briefly outlined in the following paragraphs.

The NJOY-2012 code is comprised of a variety of packages that each perform separate manipulations on the nuclear data. For this project the RECONR, BROADR, THERMR, HEATR, GROUPR, and GAMINR modules were used. The RECONR module reconstructs the continuous-energy cross sections from the tabular data and resonance parameters found in the ENDF/B data files. The BROADR module doppler-broadens the cross sections given a material temperature; in this work, cross sections were calculated at 325K. The THERMR module creates thermal cross sections for all isotopes as free-gas nuclei and for a select list of isotopes that demonstrate lattice-scattering behavior. The HEATR module calculates kermas. Finally, the GROUPR module calculates multigroup cross sections given a specified energy group structure and weighting function. In this work the NuGET 89-group neutron structure and 48-group gamma structure were specified and one of NJOY-2012s built-in weighting functions was specified. This group structure, default option 6, contains a fusion energy spectrum, a fission energy spectrum, a 1/E slowing down region, and a thermal Maxwellian distribution (R.E. MacFarlane, 2012).

The GROUPR module generates total neutron cross sections, group-to-group scattering cross sections, and gamma-production cross sections. These cross sections are printed on a reaction-by-

reaction basis. Fission cross sections are produced for fissionable isotopes; NJOY-2012 produces fission cross sections, reports the number of neutrons produced per fission for each group, and prints a fission spectrum for the fission neutrons.

Finally, the GAMINR module produces gamma cross sections. Unlike the other NJOY modules, which are run on isotopes, the GAMINR module is run on data sets for elements.

2.3. Generation of SCEPTRE-formatted multigroup cross sections

Parsing the NJOY-2012 code output to assemble the vector of total cross sections $\sigma_{\{t,g\}}$ and the scattering matrices containing $\sigma_{\{g' \to g,l\}}$ is challenging. The code output contains tables of multigroup cross sections for all the interactions a neutron may undergo with the specified isotope. Parsing the tables of cross sections is complicated due to the use of a variety of data-presentation formats. Inconsistencies in the output formats between NJOY-2012 modules further complicated this step. For example, in some modules, a Fortran-style maximum line width limited the number of columns of data that could be presented before the data was "wrapped", while in other modules no such limit was observed. Finally, relatively exotic reactions in heavy isotopes such as (n,3n), (n,n+α), and (n,n+p) had to be manually identified and parsed.

In addition to total and scattering cross sections several cross-sections related to energy deposition may be parsed from the NJOY-2012 output. These cross sections include energy deposition, kerma, and heating.

The SCEPTRE deterministic transport code requires that a data file of multigroup cross sections be provided as a code input to read by SCEPTRE at runtime. The process to generate this multigroup data file includes:

- obtaining nuclear data as ENDF/B-VII.1 data files for each isotope of interest,
- writing an NJOY-2012 input file for each isotope,
- running NJOY-2012 on each isotope,
- post-processing the NJOY-2012 output files to assemble isotope-specific vectors of removal cross sections, matrices of scattering cross sections, and vectors of energy-deposition cross sections,
- converting the isotope-specific microscopic cross sections to material-specific macroscopic cross sections by mixing materials according to isotopic abundances and material densities,
- writing the macroscopic cross sections as a NETCDF-formatted text file, and
- converting the NETCDF-formatted text file into a NETCDF file for use by SCEPTRE.

A set of Python scripts were written for this project to accomplish most of these tasks.

3. CODE-TO-CODE COMPARISON WITH MCNP

To verify that the neutron-gamma cross sections generated with NJOY-2012 are accurate a code-to-code comparison was conducted between SCEPTRE and MCNP. While not definitive, these results suggest that for most elements the neutron-gamma cross sections generated with MCNP-2012 for use by SCEPTRE are accurate.

3.1. Model-form differences (and limitations of this analysis)

The MCNP code is a continuous-energy radiation transport code. The continuous-energy treatment of the cross sections in MCNP is more accurate than the multigroup treatment used in SCEPTRE. The MCNP calculations were performed using cross sections derived from the ENDF/B-VII.1 data sets, although they are processed differently than the cross sections used by SCEPTRE (that is, it is not clear with which version of NJOY these cross sections were generated, or if they were even generated with NJOY).

MCNP is a Monte Carlo radiation transport code which works by simulating particle histories from source until they are absorbed or leave the problem. Scalar fluxes or energy-dependent fluxes may be calculated by tallying particles during the simulation. The accuracy of these tallies is proportional to the number of histories that are simulated. For these comparisons the accuracy of the MCNP results was balanced against the time required to perform these calculations and, in many cases, statistical uncertainty is apparent in the Monte Carlo results.

The neutron and gamma energy spectra were tallied in MCNP at a specific position using tallies that matched the multigroup energy structure used in SCEPTRE. These tallies allow the continuous-energy MCNP results to be compared with the multigroup SCEPTRE results. Uncertainties in the MCNP results presented in this document were not reported but were generally small compared to the magnitude of the solutions and the solutions' accuracy was sufficient for the analysis performed in this work.

The code-to-code comparisons are presented in this work as a mix of quantitative and qualitative metrics. Although many of the results are qualitative these comparisons identified numerous bugs in the python scripts that post-process the NJOY-2012 output and write the SCEPTRE cross-section file. These mistakes included an indexing error in the NJOY-2012 output for annihilation photons, a mistake in the python post-processing scripts that neglected the fission cross sections for thorium and uranium, and a miscommunication of the Legendre polynomial cross sections as they were passed to SCEPTRE.

The error in the cross-sections associated with the Legendre moments representing anisotropic scattering was particularly difficult to find. The scattering source term in the Boltzmann transport equation is constructed by expanding the anisotropic scattering in the Legendre polynomials. These terms include a division by $(2l + 1)$, where l is the scattering order. This division may be performed in either the cross-section preparation tool or within the deterministic transport code. SCEPTRE expects the cross-section-data file to contain cross sections that have not yet been divided and performs this division at run-time. The python post-processing script also

performed this division, leading to errors in the SCEPTRE results. Note that this error does not appear for isotropic scattering ($l = 0$), which dominates many neutron interactions.

3.2. Problem description

A one-dimensional problem was defined to compare SCEPTRE and MCNP results. This problem was designed to minimize the differences between the deterministic SCEPTRE code, which discretizes the space, angle, and energy variables, and the Monte Carlo code MCNP, which is continuous in space, angle, and energy. The goal of this test problem was to identify errors in the scripts which set up and run NJOY-2012 and then postprocess the output to extract cross sections for SCEPTRE. A quick resolution study was used to choose a space- and angle-mesh that was sufficiently resolved to suppress discretization errors in those variables. The energy mesh was chosen to use the group structure used by the Sandia code NuGET. Differences in the solutions generated by SCEPTRE and MCNP for an extremely simple problem should be traceable to errors in the cross-section data used in SCEPTRE.

The ideal method to verify that the python scripts used to post-process the NJOY-2012 output accurately collect the multigroup cross sections would be to compare the vector of removal cross sections and matrices of scattering cross sections value-by-value to those created by a trusted cross-section generation code. Without this capability a code-to-code comparison of radiation transport results calculated for a simple problem is used to identify elements for which the cross-section data is suspect. The nature of error in the SCEPTRE results (e.g., under- or over-prediction of the scalar flux or errors in specific portions of the energy spectra) and the materials which show disagreement (e.g., all materials, or just fissionable elements) were used to inform the debugging process.

The simple test problem examined in this work contained a homogeneous material. The problem was run for all stable elements on the periodic table. NJOY-2012 was run on every stable isotope found on the chart of the nuclides and then mixed according to natural abundances to form natural elements. Finally, each element was converted from microscopic cross sections (in units of cm^2) to macroscopic cross sections (in units of 1/cm) as used by SCEPTRE using the nominal density if each element. Elements which are naturally gasses were processed with artificial densities of 1 g/cm^3. This process results in a very large SCEPTRE cross-section file containing all stable elements on the periodic table.

The SCEPTRE geometry described a one-dimensional slab of homogeneous material defined by x-coordinates. The NuGET 89-energy-group neutron group structure and 48-energy-group gamma group structures were used, with one minor modification: a narrow (20-eV) group was added around 14.0 MeV to serve as an approximate mono-energetic source group. A unit (1 particle/cm^2) boundary source of neutrons was applied to the left face of the slab; this source was isotropic in angle and present in the narrow group centered at 14.0 MeV. No external source of gamma rays was applied to these problems. Gamma radiation was produced by neutron scattering and neutron absorption interactions within the problem. The slab was 20cm in length and solved in SCEPTRE with 100 evenly-spaced spatial cells.

The MCNP geometry consisted of a two-dimensional cylinder with its major axis along the x-direction and its minor direction along the y-axis. Reflective boundary conditions were applied to the surface parallel to the cylinder's major axis. A unit (1 particle/cm^2) boundary source of 14.0 MeV neutrons were applied to the left end of the cylinder. A vacuum boundary condition was applied to the right face of the cylinder.

Four quantities of interest were extracted from the problem solutions. The scalar flux as a function of position was extracted for both the neutrons and gamma particles. The SCEPTRE results present the average scalar flux value in each spatial cell. Although the MCNP solution was calculated without discretizing in space, the scalar flux was tallied over discrete lengths along the major axis of the cylinder. The tally "mesh" used for the MCNP results was noticeably finer than the SCEPTRE spatial mesh. Absolute and relative errors in the SCEPTRE results were computed at the midpoints of each MCNP tally cell by linearly interpolating the SCEPTRE results across the spatial cells used in the deterministic calculation.

The spectrum of the neutrons and gamma particles at a specific point in space was calculated with both SCEPTRE and MCNP. The SCEPTRE solution represents the scalar flux as piecewise-constant in energy, according to the multigroup energy structure. The continuous-energy MCNP solution was tallied in energy using tallies corresponding to the group structure used by SCEPTRE. These spectra were tallied in a small tally cell located at a depth of 5.0cm into the slab. The SCEPTRE results represent the energy solution in the spatial cell spanning 5.0 to 5.2cm in the slab.

The SCEPTRE scalar flux solutions may include discretization errors due to the space, energy, and angle discretizations. While the MCNP scalar flux solution does not contain discretization errors it will contain Monte Carlo uncertainty. For these results the uncertainty in the MCNP results is not presented; rather, the MCNP calculations were run until the noise in the MCNP solution was "small" compared to the solution.

The energy-integrated scalar neutron and gamma fluxes were plotted versus position to compare the SCEPTRE and MCNP results. Similarly, the energy spectra of the neutrons and gamma particles at a fixed position were plotted to compare the SCEPTRE and MCNP results. These qualitative comparisons were sufficient to inform the debugging of the python scripts used to post-process the NJOY-2012 output. In addition to these code-to-code comparisons, manual hand-checking of the cross-section-data file handed to SCEPTRE was performed to compare cross-section values in that file to the values reported in the NJOY-2012 output files. This laborious process was performed for several elements for which the results of the code-to-code comparison were unsatisfactory to rule out errors in the python post-processing scripts.

Several elements were not included in this analysis. Elements with no stable isotopes were excluded. Other elements were excluded due to a lack of nuclear data; in several cases, neither the LANL nuclear information service nor the IAEA nuclear data service included cross section data for particular elements (International Atomic Energy Agency Nuclear Data Services, 2019) (Los Alamos National Laboratory T-2 Nuclear Information Service, 2019). Finally, in one case, an algorithmic shortcoming precluded the SCEPTRE transport code from solving the problem of interest. These special cases are summarized in Table 1: Elements excluded from analysis.

SCEPTRE was not able to produce a solution for a 20cm slab of hydrogen with a density of $1 g/cm^3$. Pure hydrogen has a scattering ratio very close to 1.0; that is, the ratio of the scattering cross section to the total cross section is very close to unity across all energies. For a nearly-infinite slab of hydrogen a source-iteration algorithm (as used by SCEPTRE) would require an extremely large number of iterations to converge to the solution of the problem. Problems of this nature may be solved using one of several acceleration schemes, including DSA and Krylov acceleration schemes, but these methods are not implemented in SCEPTRE. The algorithms have not been implemented in SCEPTRE because they are not useful acceleration schemes for the highly anisotropic scattering found in the photon-electron transport problems to which SCEPTRE is usually applied.

Table 1: Elements excluded from analysis.

Excluded Element	Reason
Hydrogen (z=1)	SCEPTRE algorithm unable to converge solution.
Technetium (z=43), Promethium (z=61), Polonium (z=84) through Actinium (z=89), transuranics (z > 92)	Not naturally-occurring; no stable isotopes.
Nitrogen (gamma) (z=7)	Nuclear data for gamma production missing.
Neon (z=10), Ytterbium (z=70), Osmium (z=76), Platinum (z=78)	Lack of nuclear data.

3.3. Results

Results are presented for two different quantities of interest. The first, the scalar flux in units of particles per cm^2-s, is plotted as a function of position within the slab. The second, the energy spectra in units of particles per cm^2-MeV-s and in units of particles per cm^2-s, is plotted at a depth of 5cm within the slab.

3.3.1. Scalar flux results

In general, the agreement between the SCEPTRE- and MCNP-generated scalar-flux solutions varied between very good and excellent, with a notable series of exceptions in the first row of transition metals from titanium (z=22) to zinc (z=30). The elements showing significant error were titanium, vanadium, chromium, manganese, iron, cobalt, nickel, copper, and zinc. Extensive effort was invested looking for a mistake in the post-processing script for these elements because of the common nature of many of these elements. Eventually, cross sections were compared by hand-

calculating them from the NJOY-2012 output and comparing these values to the cross sections as written for use by SCEPTRE to rule out an error in the Python scripts.

The average error in the SCEPTRE scalar flux as a function of position (as compared to the MCNP solution) is plotted by atomic number in Figure 3. This plot contains the absolute error in the SCEPTRE results and is therefore uninformative without context regarding the magnitude of the scalar flux solutions. Figure 4 presents the relative error in the SCEPTRE results as compared to the MCNP solution. A disadvantage of the relative presentation becomes apparent when the two figures are compared: although the relative error in the gamma scalar flux appears quite large for several mid-z elements, the absolute magnitude of the error in the gamma scalar flux reveals that these problems have very small gamma components.

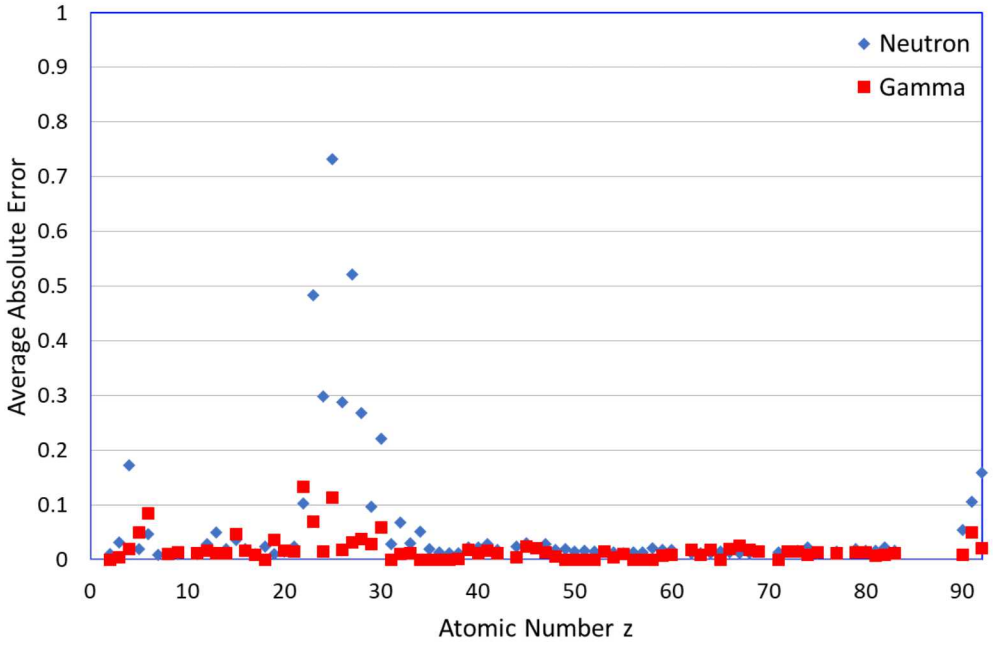

Figure 3: Absolute error in SCEPTRE scalar-flux results.

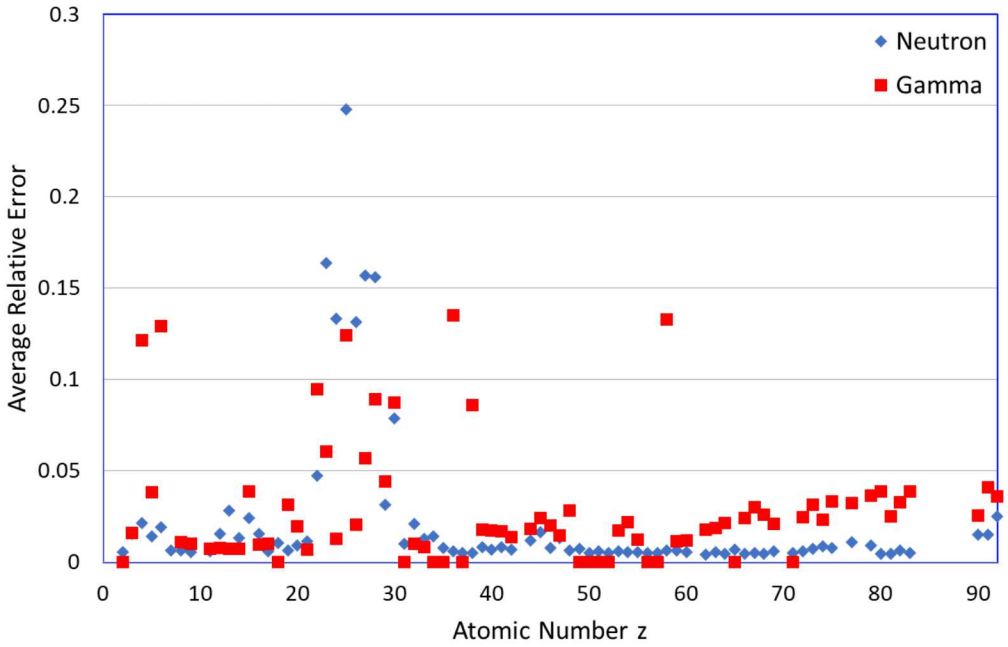

Figure 4: Relative error in SCEPTRE scalar-flux results.

The average relative errors in the neutron populations plotted in Figure 3 demonstrate excellent agreement between the SCEPTRE and MCNP solutions for most elements. Many elements demonstrate average errors of less than 2% and another handful of elements showed average errors greater than 2% but less than 5%. The first row of transition metals, containing the elements titanium (z=22) through zinc (z=30), showed poor agreement between the SCEPTRE and MCNP neutron scalar flux results.

The errors in the gamma populations plotted in Figure 3 and Figure 4 demonstrate excellent agreement in the SCEPTRE and MCNP solutions. Significant error in the gamma solutions was identified in carbon (z=6) and in the transition metals titanium (z=22) through zinc (z=27). As the problem contained no external source of gamma radiation, the errors in the gamma solutions for the transition metals are likely directly related to the errors in the neutron solutions. Although large relative errors in the gamma solutions are apparent for several mid-z elements, the magnitude of the scalar flux of gammas in these problems was quite small, and the accuracy of the MCNP tallies for these very small values is not clear.

Three examples of the plots comparing MCNP and SCEPTRE scalar flux solutions are presented in this section. Figure 5, Figure 6, and Figure 7 illustrate excellent (error approximately 2%), good (error approximately 5%), and poor (large error) agreement between the MCNP and SCEPTRE results, respectively. Note that statistical uncertainty in the Monte Carlo solutions are visible as apparent noise in the MCNP scalar flux solutions.

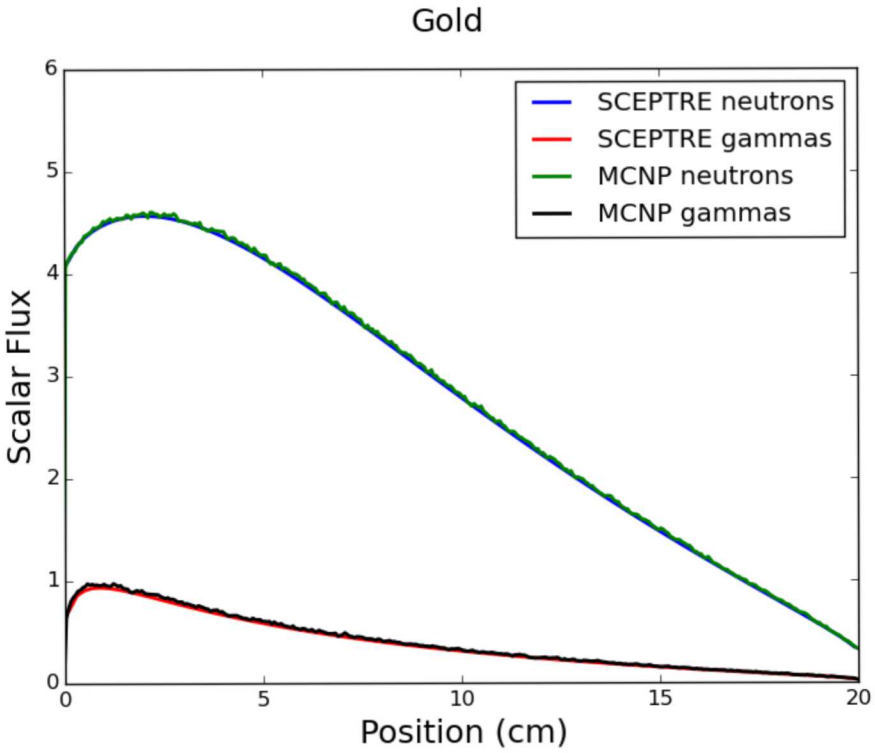

Figure 5: Scalar flux solution for gold (z=79) demonstrating excellent agreement between the SCEPTRE and MCNP neutron and gamma results.

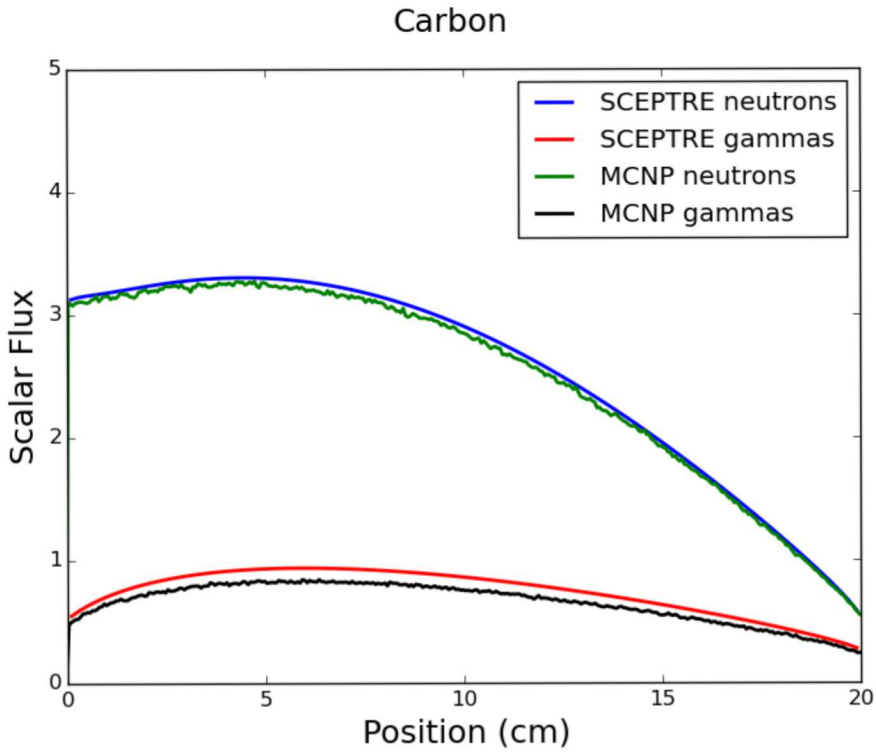

Figure 6: Scalar flux solution for carbon (z=6) demonstrating good agreement between the SCEPTRE and MCNP neutron results.

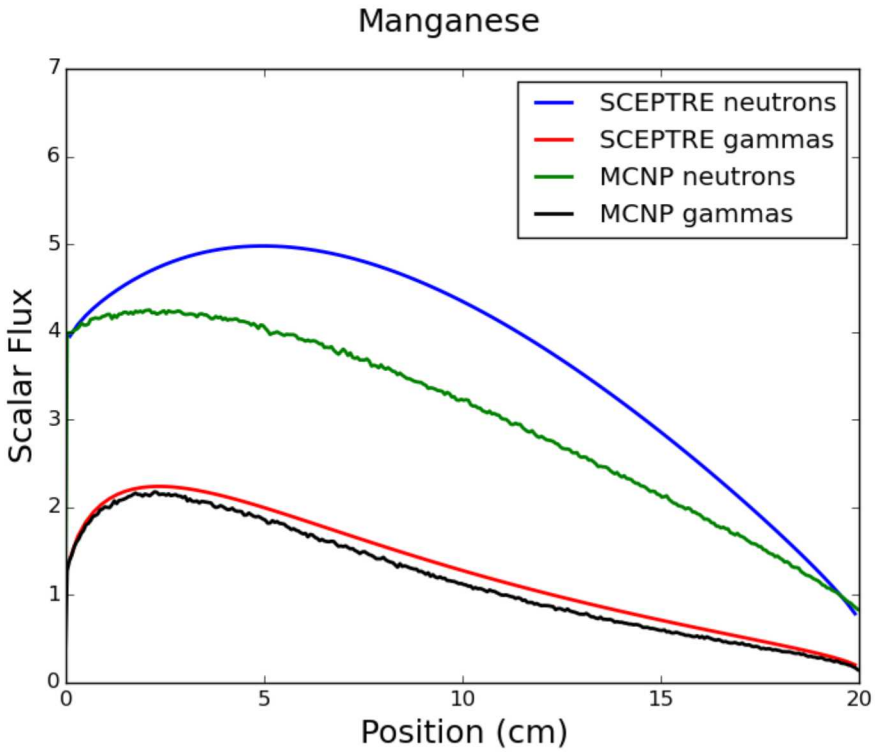

Figure 7: Scalar flux solution for manganese (z=25) demonstrating poor agreement between the SCEPTRE and MCNP neutron results.

3.3.2. Energy spectra results

Two different methods of visualizing the energy spectra within the slab are presented in this section. The first, a differential-energy spectra, plots the energy spectra with units of particles per unit area per unit time per unit energy, p / (cm^2-s-MeV). The second, an integral-energy spectra, presents the energy spectra with units of particles per unit area per unit time, p / (cm^2-s). The SCEPTRE scalar fluxes presented in the previous section are calculated in each spatial cell by summing the integral energy spectra across all energy groups or by integrating the differential energy spectra across all energy groups.

Energy spectra are presented for gold, carbon, and manganese in this section. These figures correspond to the excellent, good, and poor agreement in the scalar flux results between MCNP and SCEPTRE illustrated in the previous section.

The continuous-energy neutron cross sections are also plotted for these three materials in this section. These materials were chosen to present in these sections because gold and manganese are mono-isotopic and carbon, while composed of two isotopes, is available as a natural material from the Los Alamos Nuclear Information Service. In these three cases the cross sections for natural material may be presented with a single figure.

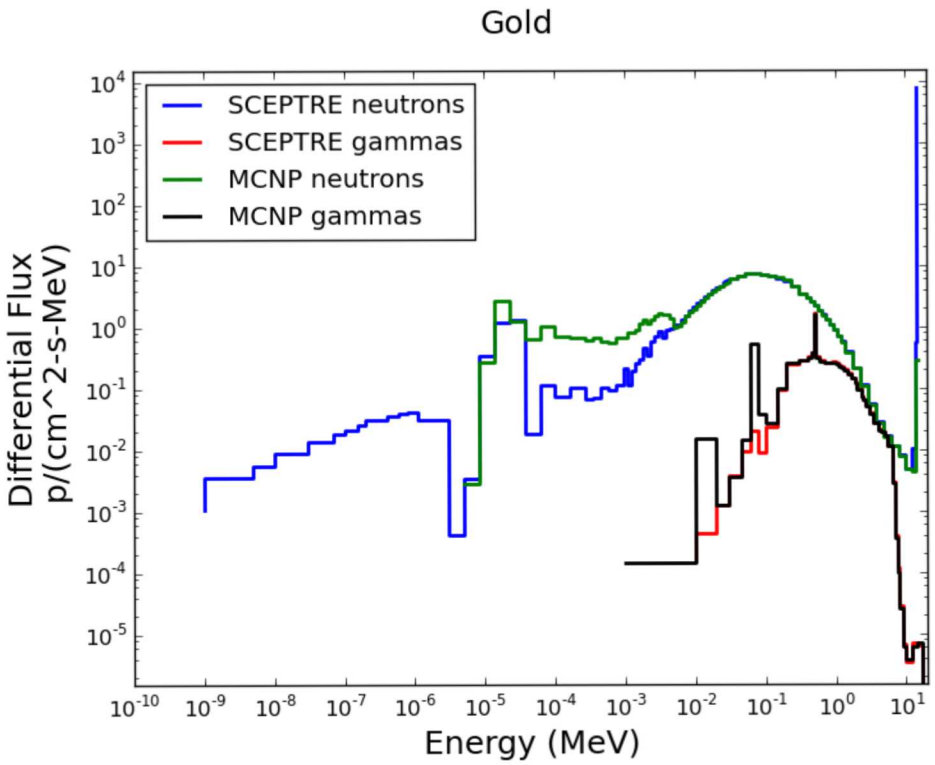

Figure 8: Differential energy spectra for gold (z=79) at 5cm.

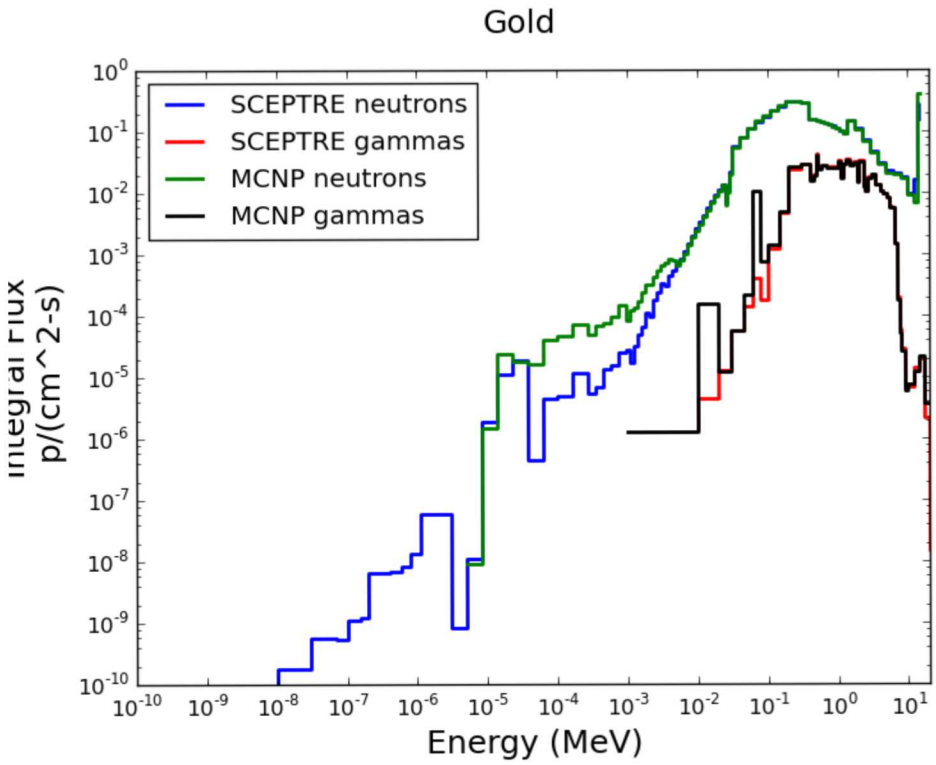

Figure 9: Integral energy spectra for gold (z=79) at 5cm.

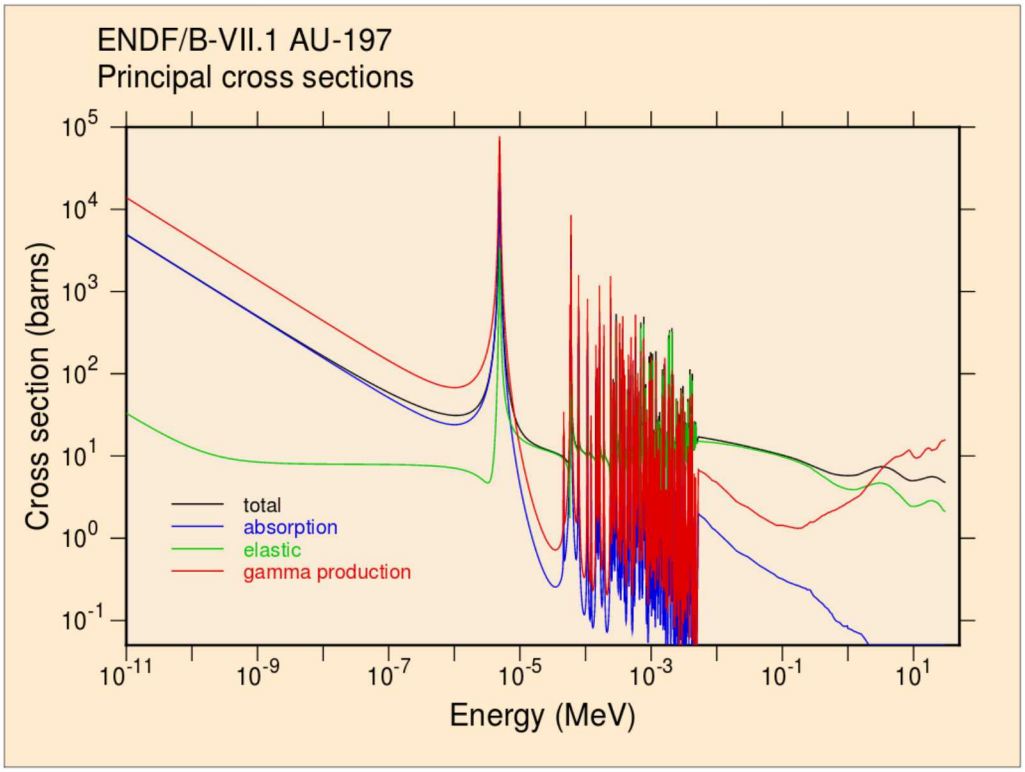

Figure 10: Microscopic cross section for gold (z=79, 100% Au-197). (Los Alamos National Laboratory T-2 Nuclear Information Service, 2019)

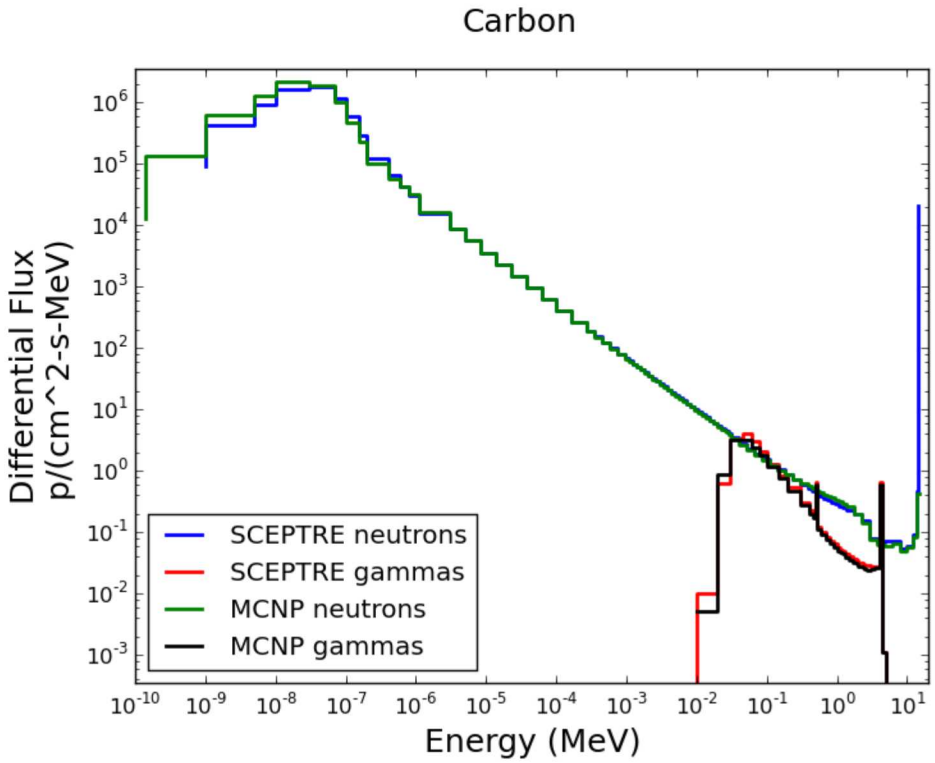

Figure 11: Differential energy spectra for carbon (z=6) at 5cm.

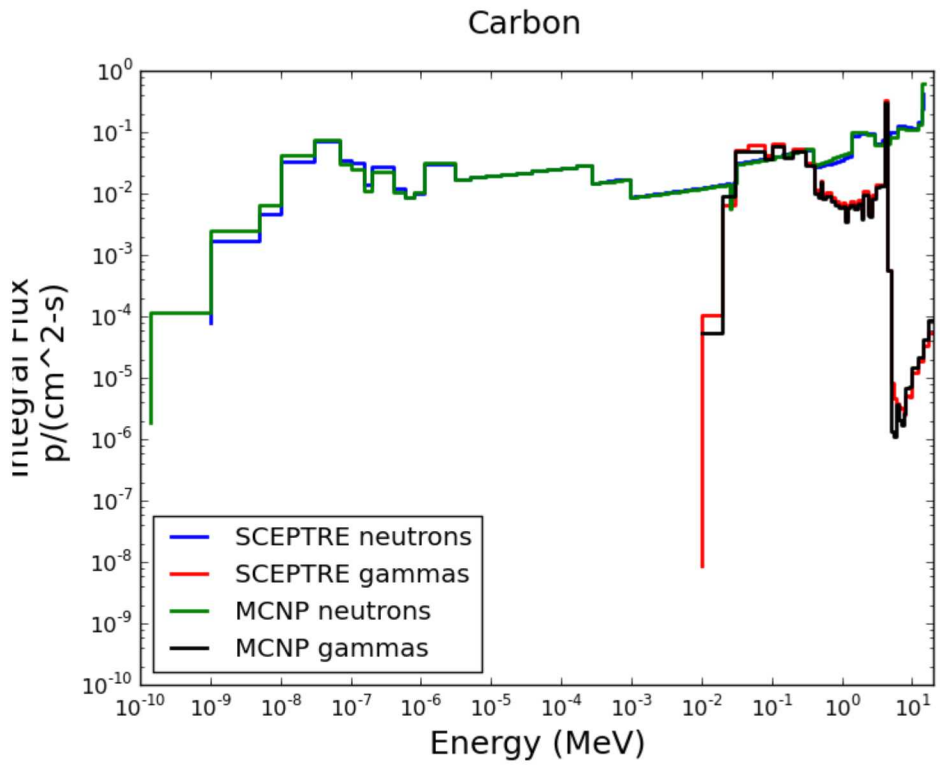

Figure 12: Integral energy spectra for carbon (z=6) at 5cm.

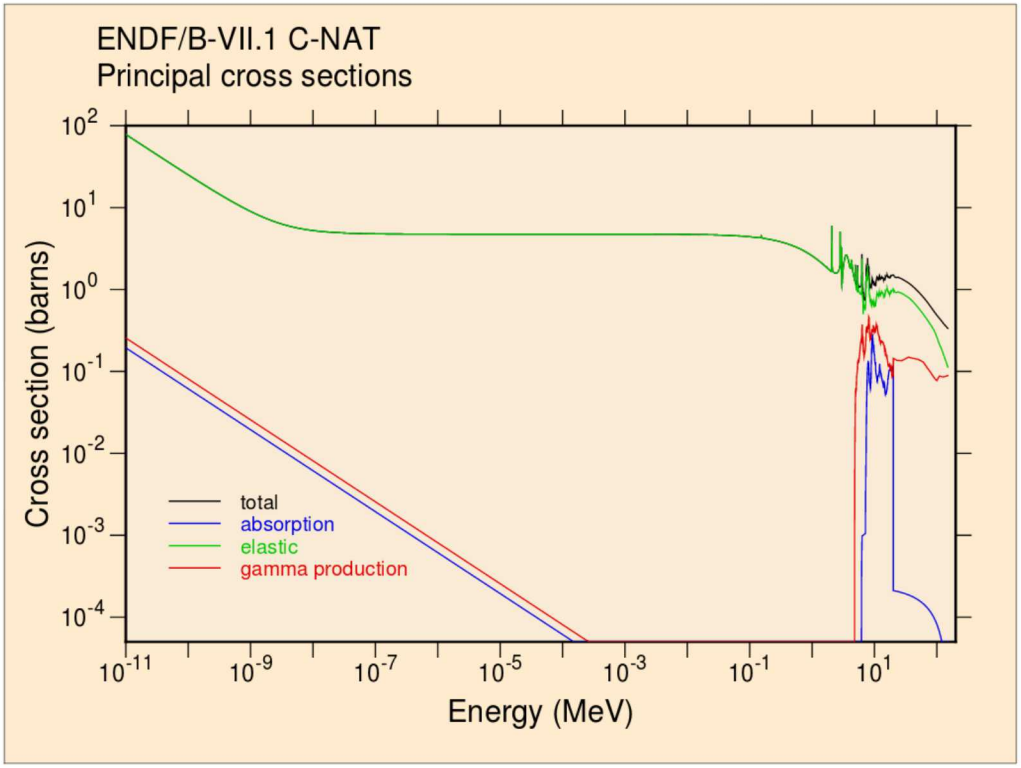

Figure 13: Microscopic cross sections for carbon (z=6, natural isotopics). (Los Alamos National Laboratory T-2 Nuclear Information Service, 2019)

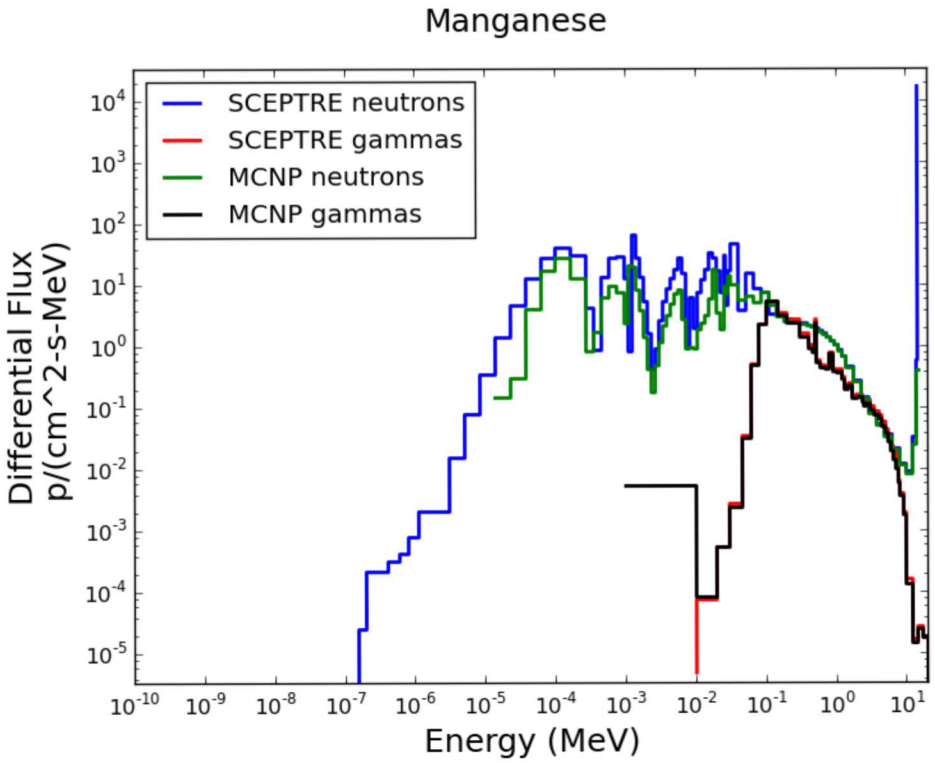

Figure 14: Differential energy spectra for manganese (z=25) at 5cm.

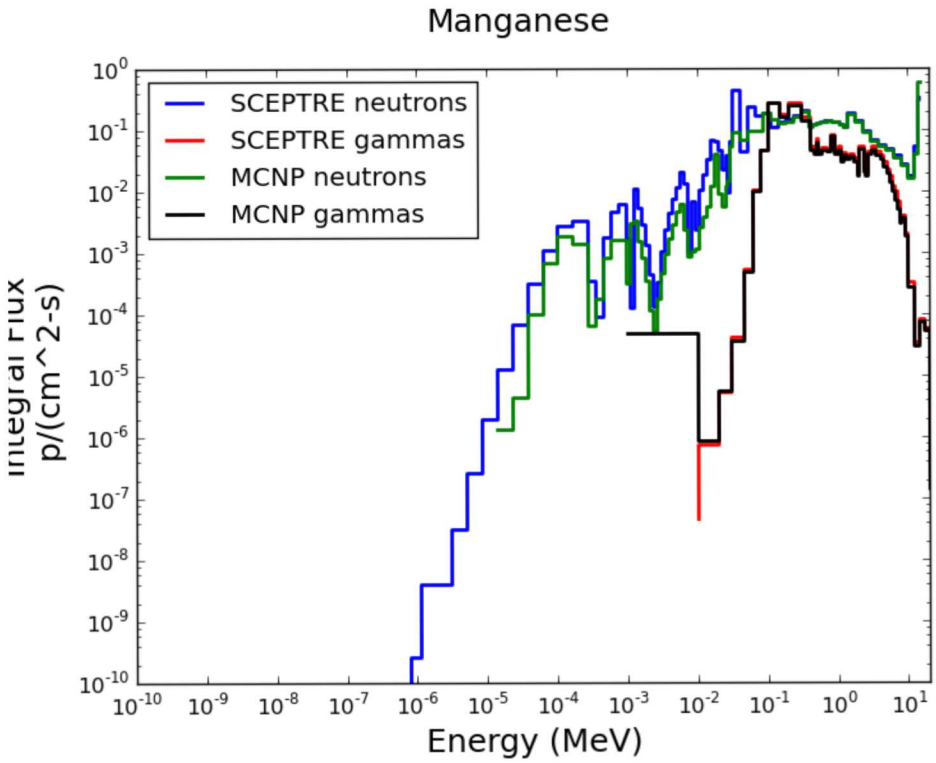

Figure 15: Integral energy spectra for manganese (z=25) at 5cm.

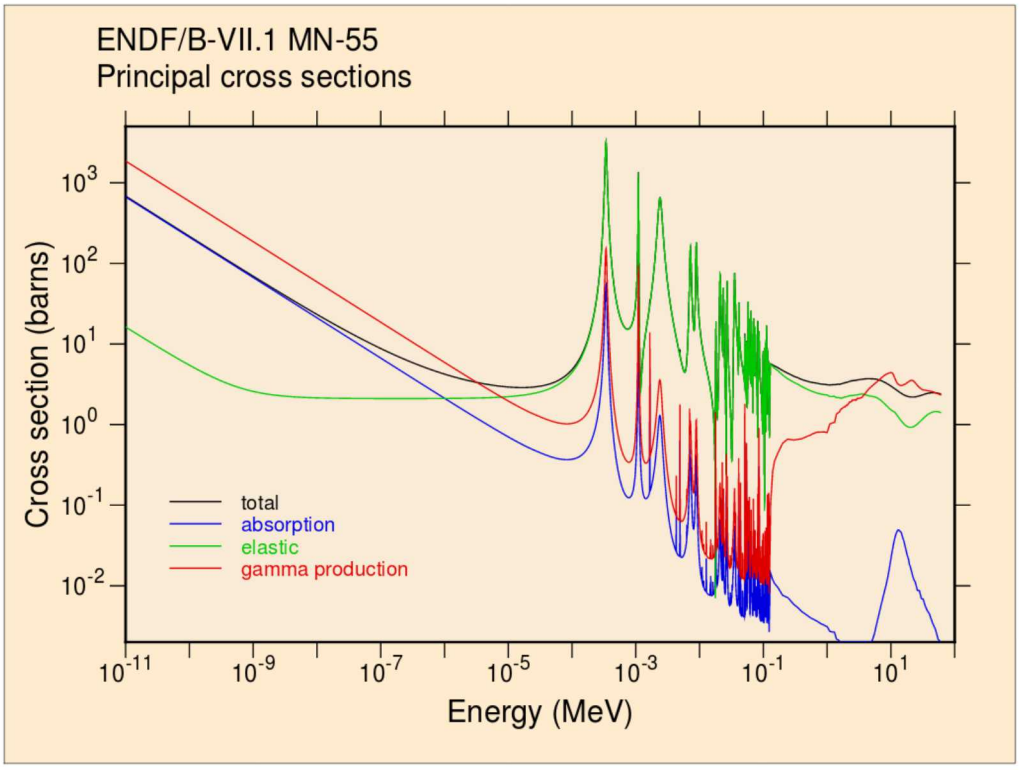

Figure 16: Microscopic cross sections for manganese (z=25, 100% Mn-55). (Los Alamos National Laboratory T-2 Nuclear Information Service, 2019)

3.3.3. *Interpretation of the computational results*

The results presented in the previous several sections lead to several general conclusions. For nearly all elements on the periodic table, the SCEPTRE calculations using cross sections generated by NJOY -2012 and processed by python scripts written for this project yield excellent agreement with continuous-energy MCNP calculations. A series of notable exceptions are found in the first row of the transition metals with atomic numbers between 22 and 30.

A close examination of the plots comparing the energy spectra calculated with MCNP and SCEPTRE strongly suggest that the SCEPTRE calculations are not accurately modeling neutron behavior in the resolved-resonance region of the energy spectra. Both the gold and manganese energy spectra calculated with SCEPTRE begin showing significant departures from the MCNP-calculated spectra at the energy at which the cross sections transition from the unresolved-resonance region to the resonance region. In both cases SCEPTRE the cross sections generated with NJOY-2012 lead to an under-estimation of neutron absorption as neutrons downscatter across the resolved-resonance region of the energy range. This causes SCEPTRE to over-estimate the number of neutrons that reach the low-epithermal and thermal energy ranges, inflating the scalar flux.

Our current hypothesis regarding the error in the SCEPTRE results calculated for the first row of the transition metals is that in these metals the transition from the unresolved-resonance region to the resolved-resonance region happens at relatively high energy. The magnitude of the error in the scalar flux appears to be directly correlated to the energy at which this transition occurs and the

number of neutrons that reach that transition energy before being absorbed or leaking from the problem. This transition from unresolved-resonances to resolved-resonances occurs in manganese at an energy approximately an order of magnitude larger than the transition energy in gold. A much greater fraction of the total number of neutrons in the energy spectra are at energies below this transition energy in manganese than in gold.

The plots of energy spectra reveal why the error in the SCEPTRE gamma scalar flux results tends to be much smaller than the error in the neutron scalar flux results for the first row of transition metals. Gamma rays are generated through inelastic scattering at high neutron energies and by absorption reactions that primarily occur at low neutron energies. The differential- and integral-energy spectra for manganese show excellent agreement at high neutron energies. The population of neutrons at low energy is orders of magnitude smaller than the population of high-energy neutrons. This supports the conclusion that most of the gamma rays are generated by high-energy neutron inelastic scattering events in an energy regime that SCEPTRE accurately models.

4. CONCLUSIONS

The goal of this project was to produce multigroup coupled neutron-gamma cross sections with the cross-section preparation code NJOY-2012 for use by the deterministic radiation transport code SCEPTRE. Python scripts were written to download ENDF/B-VII.1 cross-section data files from Los Alamos' Nuclear Information Services website, write input decks for NJOY-2012, run NJOY-2012, post-process the NJOY-2012 output to assemble vectors of removal cross sections and matrices of scattering cross sections, and finally to write the multigroup cross sections in the format expected by SCEPTRE.

Extensive code-to-code comparisons were performed with the continuous-energy radiation transport code MCNP. These calculations suggest that for most elements SCEPTRE calculations performed using the NJOY-2012 cross sections yield very accurate solutions, although caution must be applied if the quantity of interest is specific to low-energy neutrons. The SCEPTRE results for elements with atomic numbers between 22 (titanium) and 30 (zinc) showed significant error.

The error in the low-z transition metals was traced to the portion of the energy range corresponding to the resolved resonances. SCEPTRE, using the NJOY-2012 cross sections, underestimates absorption in the resonance regions for most elements. This effect is particularly pronounced for these low-z transition metals which have relatively high transition energies between the resolved-resonance region and unresolved-resonance region of the cross-section data. Further investigation into this behavior is needed to understand and correct this source of error

REFERENCES

Duderstadt, J. J. (1976). *Nuclear Reactor Analysis.* John Wiley & Sons.

E. E. Lewis and W. F. Miller, J. (1993). *Computational Methods of Neutron Transport.* La Grange Park, Illinois: American Nuclear Society.

International Atomic Energy Agency Nuclear Data Services. (2019, 5 10). *Evaluated Nuclear Data File (ENDF) Standard Request*. Retrieved from https://www-nds.iaea.org/exfor/endf.htm

Los Alamos National Laboratory T-2 Nuclear Information Service. (2019, 5 10). *ENDF/B_VII.1 Incident-Neutron Data*. Retrieved from https://t2.lanl.gov/nis/data/endf/endfvii.1-n.html

National Institute of Standards and Technology Physical Measurement Laboratory. (2019, 5 10). *XCOM: Photon Cross Sections Database*. Retrieved from https://physics.nist.gov/PhysRefData/Xcom/html/xcom1.html

R.E. MacFarlane, e. a. (2012). *The NJOY Nuclear Data Processing System, Version 2012.* Theoretical Division. Los Alamos: Los Alamos National Laboratory.

DISTRIBUTION

Email—External (encrypt for OUO)

Name	Company Email Address	Company Name
Benedict Campbell	bjcampb@sandia.gov	Atomic Weapons Establishment

Email—Internal

Name	Org.	Sandia Email Address
Don Bruss	01341	dbruss@sandia.gov
Clifton Drumm	01341	crdrumm@sandia.gov
Wesley Fan	01341	wcfan@sandia.gov
Shawn Pautz	01341	sdpautz@sandia.gov
Matthew Sternat	01384	mrstern@sandia.gov
Lawrence Sanchez	08845	lcsanch@sandia.gov
Technical Library	01177	libref@sandia.gov

Sandia National Laboratories

Sandia National Laboratories is a multimission laboratory managed and operated by National Technology & Engineering Solutions of Sandia LLC, a wholly owned subsidiary of Honeywell International Inc. for the U.S. Department of Energy's National Nuclear Security Administration under contract DE-NA0003525.